Calibrating Double-Loop H-Field Probe Measurements of RF Coil Current for MRI

Wang, Wenjun; Sánchez-Heredia, Juan Diego; Maurouard, Tom; Zhurbenko, Vitaliy; Ardenkjær-Larsen, Jan Henrik

Published in:
IEEE Journal of Electromagnetics, RF and Microwaves in Medicine and Biology

Link to article, DOI:
10.1109/JERM.2023.3274742

Publication date:
2023

Document Version
Peer reviewed version

Calibrating double-loop H-field probe measurements of RF coil current for MRI

Wenjun Wang, Juan Diego Sánchez-Heredia, Tom Maurouard, Vitaliy Zhurbenko, and Jan Henrik Ardenkjær-Larsen

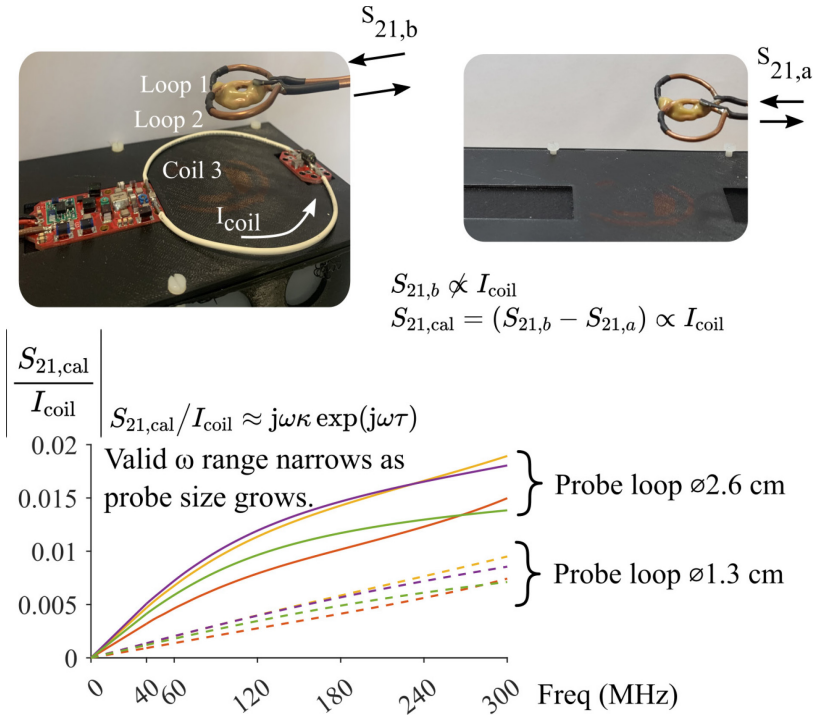

A double-loop H-field probe is used to measure current on RF coils for MRI. Direct S parameter measurement, denoted by $S_{21,b}$, is not proportional to coil current. After subtracting the coil-free S parameter, $S_{21,a}$, the quantity $S_{21,\mathrm{cal}} = S_{21,b} - S_{21,a}$ is proportional to coil current. The ratio $|S_{21,\mathrm{cal}}/I_{\mathrm{coil}}|$ is plotted for several setups of different probe size, different coil size and different coil-to-probe distance. For double-loop H-field probes of ⌀1.3 cm probes and coil-to-probe distance no less than 5 cm, there is $S_{21,\mathrm{cal}}/I_{\mathrm{coil}} \approx \mathrm{j}\omega\kappa \exp(\mathrm{j}\omega\tau)$ up to 300 MHz, where $\kappa < 0$ and $\tau < 0$ are setup-specific constants.

Take-Home Messages

- Measurement of MRI coil current by a double-loop H-field probe can be calibrated to improve sensitivity and remove crosstalk interference.
- Calibrated S_{21} measurement is proportional to coil current, and up to a cut-off frequency different amongst setups, $S_{21} \approx I_{\mathrm{coil}} \times \mathrm{j}\omega\kappa \exp(\mathrm{j}\omega\tau)$, where $\kappa < 0$ and $\tau < 0$ are setup-specific constants, which is demonstrated by two probes of ⌀1.3 cm and ⌀2.6 cm loops up to 300 MHz.
- This fast calibration technique widens the dynamic range, enables accurate measurement of coil current, thereby expediting MRI coil building.
- It is for the first time proven that the calibrated S_{21} measurement is proportional to coil current, and knowing $S_{21} \approx I_{\mathrm{coil}} \times \mathrm{j}\omega\kappa \exp(\mathrm{j}\omega\tau)$ allows fairly comparing coil current in a frequency band or at several frequency points.

Calibrating double-loop H-field probe measurements of RF coil current for MRI

Wenjun Wang, Juan Diego Sánchez-Heredia, Tom Maurouard, Vitaliy Zhurbenko, and Jan Henrik Ardenkjær-Larsen

Abstract: **Objective:** Double-loop H-field probes are often used to measure current on loop antennae for magnetic resonance imaging (MRI). Loop crosstalk limits the dynamic range of direct measurements with such probes. The crosstalk can be removed by simple calibration. This work analyses the quantitative relation of a probe's calibrated S_{21} with the RF coil current. **Method:** The analytical relation between RF coil current and calibrated S_{21} measurements of a probe is established with the multi-port network theory, and verified by full-wave simulation and benchtop measurements. The effect of calibration is demonstrated by measuring the ^{1}H trap frequency, the active detuning, and the preamplifier decoupling. **Results:** The calibration removes the effect of crosstalk in a probe and improves the lower bound of $|S_{21}|$. The calibrated S_{21} is proportional to coil current. In the lower frequency range, the ratio of calibrated S_{21} to coil current changes almost linearly with frequency. **Impact**: The calibration method improves the sensitivity of probe measurements and facilitates fine-tuning current-suppressing circuits like active detuning circuits, traps, preamplifier decoupling. The linear frequency dependency between S_{21} measurements and coil current allows easy, fair comparison of coil current up to 128 MHz, and in some cases 298 MHz, helping build multi-nucleus coils.

Keywords — probes, coils, calibration, current measurement, magnetic resonance imaging**.**

I. Introduction

Double-loop H-field probes (referred to as "probes" hereafter) are widely used to measure current on loop antennae (often called "coils") in magnetic resonance (MR) imaging [1], [2]. A probe is connected to a two-port vector network analyser (VNA), and the scattering parameter S_{21} or S_{12} reading is believed to be proportional to the current flowing on a loop coil [1]. One way to construct a probe is to overlap two loops. Other ways to construct the probe include separating the two loops far away, or arranging two loops orthogonally [3]. In any way, the purpose is to minimise the mutual inductance between the two loops. Ideally, the mutual inductance should be zero. However, this ideal case is seldom reached in practice. The most common case is that residual crosstalk exists between the loops, and the crosstalk limits the probe's sensitivity and measurement accuracy. For example, during measurement of active detuning where the RF current on the receiving MR coils is hardly detectable, the S_{21} measured is often overwhelmed by the crosstalk.

To remove the effects of the crosstalk, a simple calibration procedure can be used. A typical measurement setup is shown in Fig. 1:

1. Connect a probe to a VNA. Make sure all cable connections are tight and the setup is mechanically stable. During the measurements, put the probe far enough from the coil under test so that the double loop does not influence the coil performance; for example, the probe shall not degrade coil Q-factor or detune a resonant coil conspicuously [3]. Meanwhile, the probe should be far enough from the sample so that sample loading has negligible effects on the probe and the coil-probe interaction.
2. Remove the coil under test. The result is better if the sample remains, but removing both the coil and the sample is acceptable; choose that which is convenient. Record $S_{21,a}$.
3. Place the coil in the measurement setup. If the sample was removed in step 2, move it back. Record $S_{21,b}$.
4. Take $S_{21,\mathrm{cal}} = S_{21,b} - S_{21,a}$ (complex-number operation).

Simple as the procedure seems, how calibrated $S_{21,\mathrm{cal}}$ relates to the current on coils-under-test remains unclear.

In this article, we show that the calibrated $S_{21,\mathrm{cal}}$ is proportional to the current on the coil I_{coil}, i.e., $S_{21,\mathrm{cal}} \propto I_{\mathrm{coil}}$. We derive the ratio $K(\mathrm{j}\omega) = S_{21,\mathrm{cal}}/I_{\mathrm{coil}}$, and show that, in a lower frequency range, when the two loops in the probe are of the same size, $K(\mathrm{j}\omega)$ can be approximated by $K(\mathrm{j}\omega) \approx$

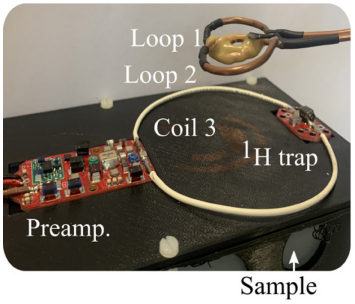

Fig. 1. A photograph of a typical test setup consisting of a probe (loop 1 and loop 2) and coil 3. The ^{1}H trap is installed to avoid interfering with ^{1}H imaging. This setup is used to test preamplifier decoupling, active detuning and ^{1}H trap frequency.

This work was supported in part by the Danish National Research Foundation DNRF 124.

Wenjun Wang is with the National Space Institute, Technical University of Denmark, 2800 Kongens Lyngby, Denmark.

Juan Diego Sánchez-Heredia is with the Department of Health Technology, Technical University of Denmark, 2800 Kongens Lyngby, Denmark.

Tom Maurouard is with CESI École d'Ingénieurs, 76000 Rouen, France.

Vitaliy Zhurbenko is with the National Space Institute, Technical University of Denmark, 2800 Kongens Lyngby, Denmark. (e-mail: vizh@dtu.dk).

Jan Henrik Ardenkjær-Larsen is with the Department of Health Technology, Technical University of Denmark, 2800 Kongens Lyngby, Denmark.

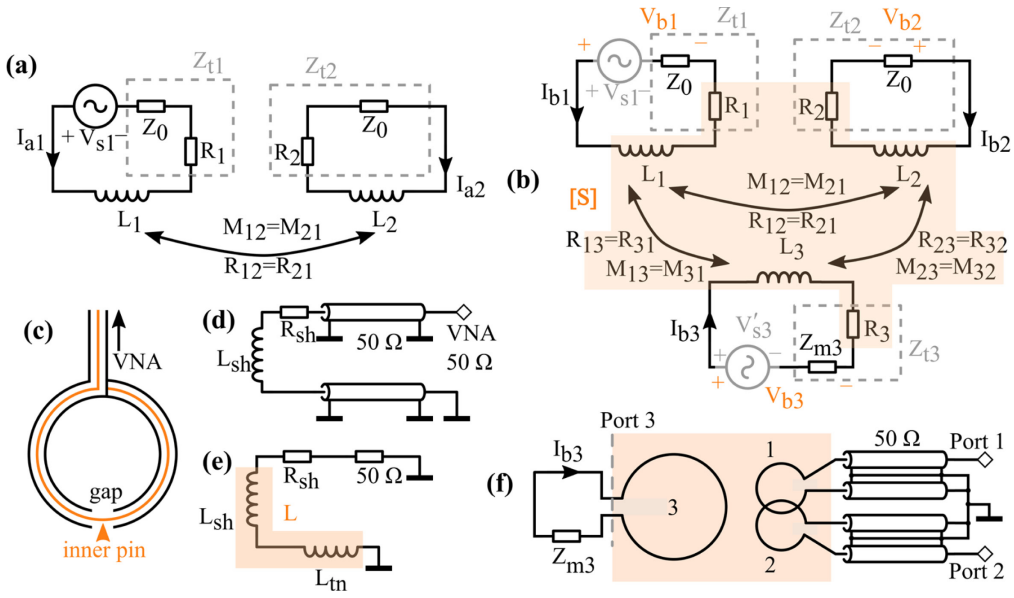

Fig. 2. (a) The circuit model of a probe. (b) A probe coupled to a coil and the circuit model. R_1, R_2 and R_3 are resistance of loops 1, 2 and coil 3. Z_{m3} is the impedance of the matching network seen by coil 3. Z_0 is the reference impedance 50 Ω. M_{12}, M_{13}, M_{23} are mutual inductance. R_{13}, R_{23}, R_{12} are mutual resistance due to e.g. sample loss. (c) A loop in a probe. (d) The equivalent circuit of (c). [7] (e) Simplified circuit of (d). A resistor R_{sh} is added on loop's outer shield to account for loss. As long as the loop is electrically small ($\beta l \ll \pi/4$), L_{sh} and L_{tn} does not change significantly with frequency. R_{sh} may vary with frequency depending on sample loading. (f) The circuit for verifying (15). The shaded region is simulated full-wave. Ports 1, 2, 3 are the ports for extracting the S parameters of the shaded area in (b).

$\mathrm{j}\omega\kappa\mathrm{e}^{\mathrm{j}\omega\tau}$, where $\kappa < 0$ and $\tau < 0$ are constants related to the particulars of a setup, e.g. positions and sizes of the coil, the sample, and the probe. The frequency limit to which $K(\mathrm{j}\omega) \approx \mathrm{j}\omega\kappa\mathrm{e}^{\mathrm{j}\omega\tau}$ holds depends on the particulars of the setup as well. The expression, however, generally works fairly well until 128 MHz. We demonstrate that, when the coil is at least 5 cm away from the probe, the frequency range extends up to 128 MHz with a probe of ⌀2.6 cm, and extends above 298 MHz with a probe of ⌀1.3 cm. We then demonstrate the effects of the calibration method on characterizing current-suppressing circuits like preamplifier decoupling networks, active detuning circuits, and ^{1}H traps. We also demonstrate how to use $|K(\mathrm{j}\omega)| \propto \omega$ to build a ^{13}C-^{23}Na coil of which the current values at the resonant frequencies of ^{13}C (30.99 MHz) and ^{23}Na (32.59 MHz) are required equal to ensure identical coil sensitivity profiles [4]. This calibration method has been shown previously to measure preamplifier decoupling accurately [5], [6].

II. Theory

The relation between calibrated S_{21} and coil current is derived under the frame of low-frequency approximation, the most essential being the quasi-static approximation (QS). For clinical MRI up to 3 T (128 MHz for ^{1}H), it is safe to use QS, to assume current values are constant along coils and the loops of probes, and to assume coils and probes do not radiate far field. For MRI up to 7 T (298 MHz for ^{1}H), with techniques like breaking coils by capacitors properly, the assumptions of constant current and no far field emission still holds firmly. Note that, for QS to hold, the perimeter of probe loops must be much less than one wavelength as well.

A. Physical Model, assumptions, and notation

A probe consists of two weakly coupled shielded loops made of coaxial cables. The working mechanisms are well described in the literature [7], [8]. An electrically small shielded loop illustrated in Fig. 2(c) can be represented by the circuit in Fig. 2(d) consisting of an inductor and two transmission line sections [7]. An electrically small ($\beta l \ll \pi/4$), shorted transmission line section can be represented as an inductor L_{tn} [9, Sec. 2.3]. The transmission line section connected to a VNA port presents $Z_0 = 50\ \Omega$ to the inductor of the loop. Therefore, a shielded loop can be represented by a resistor in series with an inductor, as shown in Fig. 2(e). A small resistor R_{sh} is included to model the loop loss.

B. Model setup

The circuit diagram of a probe in free space is illustrated in Fig. 2(a), and the diagram of a probe near a coil is illustrated in Fig. 2(b). A typical test setup to measure coil current is shown in Fig. 1. The loops are marked 1 and 2, and the coil is marked 3. We suppose that

(i) the QS approximation [10], i.e., setting the term $\partial \boldsymbol{D}/\partial t = 0$ in $\nabla \times \boldsymbol{H} = \boldsymbol{J} + \partial \boldsymbol{D}/\partial t$, well describes the coupling inside the probe and the coupling between the probe and the coil, so that the mutual interaction between loops and coils can be modelled as mutual inductance;

(ii) the interaction between loop 1, loop 2, coil 3 in Fig. 1 and Fig. 2 is reciprocal. This is guaranteed by the Lorentz reciprocity theorem [9, Sec. 1.9] as long as the space is filled with reciprocal material;

(iii) the spatial distribution of the current on coil 3, marked as I_{b3} in Fig. 2(b), is, at least, sufficiently constant along individual coil segments;

(iv) the coil is far enough from the sample, so that the coil-to-probe interaction is not heavily regulated by the sample and can be modelled as M_{12} and M_{21}; second, the coil is far enough from the probe, so that M_{12} and M_{21} are not disturbed by coil 3. This assumption follows from step 1 of the calibration procedure in Section I.

The following three additional assumptions are not needed to derive the relation between S_{21} and coil current, but they help gain insight into the frequency dependency. In practice, these three assumptions are often satisfied:

(v) the mutual resistances R_{12}, R_{21}, R_{13}, R_{31}, R_{23}, R_{32} are small. This follows from assumption (iv);
(vi) the loops of the probe have the same size, so that their inductance $L_1 = L_2$;
(vii) during a measurement, the coil is almost equally far from the two loops of the probe, so that $M_{13} \approx M_{23}$.

The loss on outer shields of loops 1 and 2 is modelled as resistance R_1 and R_2. The VNA source is modelled as a voltage source V_{s1}. The coil can be represented by an inductor and a resistor R_3, and terminated by a matching network of input impedance Z_{m3}. The coupling within the probe is modelled as mutual inductance $M_{12} = M_{21}$, and the coupling from loops to the coil is $M_{13} = M_{31}$, $M_{23} = M_{32}$. Mutual resistance due to e.g. loss in sample is $R_{12} = R_{21}$, $R_{13} = R_{31}$, $R_{23} = R_{32}$. We further introduce notations $Z_{t1} = R_1 + Z_0$, $Z_{t2} = R_2 + Z_0$, $Z_{t3} = R_3 + Z_{m3}$.

We use subscript $(\cdot)_a$ to denote quantities in Fig. 2(a), and subscript $(\cdot)_b$ to denote quantities in Fig. 2(b). We use $[\cdot]^\mathsf{T}$ for matrix transpose, and $\mathbf{1}$ for identity matrices. I_{b3} is used interchangeably with I_{coil}.

C. Voltage-current relation

Using mesh current method, the relation between the voltage V and current I in Fig. 2(a) can be written as

$$\begin{bmatrix} I_{a1} \\ I_{a2} \end{bmatrix} = \mathbf{Y}_a \begin{bmatrix} V_{s1} \\ 0 \end{bmatrix} = V_{s1} \begin{bmatrix} y_{a,11} \\ y_{a,21} \end{bmatrix}, \tag{1}$$

where

$$\mathbf{Y}_a = \mathbf{Z}_a^{-1} = \begin{bmatrix} y_{a,11} & y_{a,12} \\ y_{a,21} & y_{a,22} \end{bmatrix},$$

and

$$\mathbf{Z}_a = \begin{bmatrix} Z_{t1} + \mathrm{j}\omega L_1 & R_{12} + \mathrm{j}\omega M_{12} \\ R_{21} + \mathrm{j}\omega M_{21} & Z_{t2} + \mathrm{j}\omega L_2 \end{bmatrix}.$$

Similarly, in Fig. 2(b), there is

$$\begin{bmatrix} I_{b1} \\ I_{b2} \\ I_{b3} \end{bmatrix} = \mathbf{Y}_b \begin{bmatrix} V_{s1} \\ 0 \\ 0 \end{bmatrix} = V_{s1} \begin{bmatrix} y_{b,11} \\ y_{b,21} \\ y_{b,31} \end{bmatrix}. \tag{2}$$

where

$$\mathbf{Y}_b = \mathbf{Z}_b^{-1} = \begin{bmatrix} y_{b,11} & y_{b,12} & y_{b,13} \\ y_{b,21} & y_{b,22} & y_{b,23} \\ y_{b,31} & y_{b,32} & y_{b,33} \end{bmatrix},$$

and

$$\mathbf{Z}_b = \begin{bmatrix} Z_{t1} + \mathrm{j}\omega L_1 & R_{12} + \mathrm{j}\omega M_{12} & R_{13} + \mathrm{j}\omega M_{13} \\ R_{21} + \mathrm{j}\omega M_{21} & Z_{t2} + \mathrm{j}\omega L_2 & R_{23} + \mathrm{j}\omega M_{23} \\ R_{31} + \mathrm{j}\omega M_{31} & R_{32} + \mathrm{j}\omega M_{32} & Z_{t3} + \mathrm{j}\omega L_3 \end{bmatrix}.$$

D. Principle behind the calibration method

1) Breaking a coil amounts to removing it

Before proceeding with calculation, notice that in Fig. 2(b)'s setup, disconnecting the coil from Z_{m3} is equivalent to placing the probe in free space, i.e., the setup in Fig. 2(a). This is because if we force $I_{b3} = 0$ in (2), we have

$$\begin{bmatrix} V_{s1} \\ 0 \\ 0 \end{bmatrix} = \mathbf{Z}_b \begin{bmatrix} I_{b1} \\ I_{b2} \\ 0 \end{bmatrix} \Rightarrow \begin{bmatrix} V_{s1} \\ 0 \end{bmatrix} = \mathbf{Z}_a \begin{bmatrix} I_{b1} \\ I_{b2} \end{bmatrix}, \tag{3}$$

which, if written as $[I_{b1}, I_{b2}]^\mathsf{T} = \mathbf{Y}_a [V_{s1}, 0]^\mathsf{T}$, has the same form as (1).

2) Calculating S parameters

Let $Z_{t1} = Z_{t2} = Z_0$ and $Z_{m3} = Z_0$, where $Z_0 > 0$ is the characteristic impedance of a VNA. This value is typically 50 Ω, but not limited to 50 Ω in our derivation. Assume the S parameters of the shaded area of Fig. 2(b) are measured as

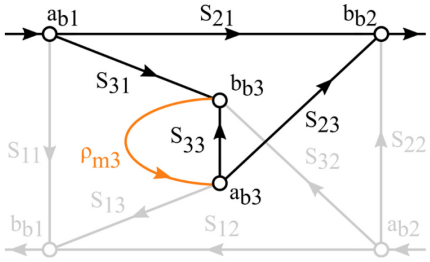

Fig. 3. The signal flow graph of Fig. 2(b).

$$\mathbf{S} = \mathbf{S}^\mathsf{T} = \begin{bmatrix} S_{11} & S_{12} & S_{13} \\ S_{21} & S_{22} & S_{23} \\ S_{31} & S_{32} & S_{33} \end{bmatrix}. \tag{4}$$

$\mathbf{S} = \mathbf{S}^\mathsf{T}$ because the setup in Fig. 2(b) is reciprocal by assumption (ii) [9, Sec. 4.3]. We keep separate notations for S_{kl} and S_{lk}, however. $\mathbf{S}$ can be visualised by a signal flow graph [9, Sec. 4.5] shown in Fig. 3. By changing $Z_{m3} = Z_0$ to an arbitrary Z_{m3}, a new signal flow $\rho_{m3} = (Z_{m3} - Z_0)/(Z_{m3} + Z_0)$ from b_{b3} to a_{b3} is added. Following the rules to simplify signal flow graphs [9, Sec. 4.5], the S_{21} under the arbitrary Z_{m3} is

$$S_{21,b} = S_{12,b} = S_{21} - \frac{S_{31}S_{23}\rho_{m3}}{S_{33}\rho_{m3} - 1}. \tag{5}$$

To calibrate, we subtract the free-space S_{21} from $S_{21,b}$. The free-space S_{21}, according to the equivalence in II.D.1), equals

$$S_{21,a} = \lim_{Z_{m3}\to\infty} S_{21,b} = S_{21} - \frac{S_{31}S_{23}}{S_{33} - 1}. \tag{6}$$

The calibrated S_{21} is

$$\begin{aligned} S_{21,\text{cal}} &= S_{21,b} - S_{21,a} \\ &= \frac{S_{31}S_{23}(\rho_{m3} - 1)}{(S_{33}\rho_{m3} - 1)(S_{33} - 1)}. \end{aligned} \tag{7}$$

The calibration method can be interpreted as follows. Before calibration, two signal paths, loop 1→loop 2 and loop 1→coil 3→loop 2, exist. Unless the induced current on the coil is strong enough, the coupling between loops 1 and 2 affects the measured $S_{21,a}$. After calibration, the effect of signal path loop 1→loop 2 is removed, and only loop 1→coil 3→loop 2 remains.

The exact ratio of calibrated S_{21} to coil current can be calculated by $K(\mathrm{j}\omega) = S_{21,\text{cal}}/I_{\text{coil}} = S_{21,\text{cal}}/I_{b3}$ with $S_{21,\text{cal}}$ specified by (7), if all S parameters in (7) and I_{b3} are known. However, (7) does not reveal the relation between $S_{21,\text{cal}}$ and I_{b3}. To reveal the relation between $S_{21,\text{cal}}$ and I_{b3}, (7) ought to be written in terms of I_{b3}, which is best expressed by voltage and impedance (or admittance). For this, it may seem straightforward to convert $\mathbf{S}$ parameters in (7) to $\mathbf{Z}$ or $\mathbf{Y}$ parameters; however, below is a method more convenient and able to incorporate the coil's circuit load.

3) Linking $S_{21,cal}$ and coil current

To derive $K(\mathrm{j}\omega)$, first, terminate coil 3 by an arbitrary circuit load Z_{m3}. By definition, $\mathbf{S}$ parameters measure the ratio of reflected wave to incident wave. We now convert

voltage and current into forward and backward waves. In the setup of Fig. 2(b), the conversion follows the form [9, Sec. 4.3], [11]

$$\begin{cases} \boldsymbol{a} = \mathbf{F}(\boldsymbol{V} + \mathbf{Z}_0\boldsymbol{I}), \\ \boldsymbol{b} = \mathbf{F}(\boldsymbol{V} - \mathbf{Z}_0\boldsymbol{I}), \end{cases} \tag{8}$$

where $\boldsymbol{a}$ is the forward wave vector, $\boldsymbol{b}$ is the backward wave vector, $\mathbf{Z}_0 = Z_0\mathbf{1}$, $\mathbf{F} = \mathbf{1} \cdot 1/\left(2\sqrt{Z_0}\right)$. Recall $S_{13} = S_{31}$; so we put a source V'_{s3} on the coil, and set $V_{s1} = 0$. Here we use $[\cdot]'$ to denote voltage, current, forward wave and backward wave produced by V'_{s3} to distinguish them from those produced by V_{s1}. Let $\boldsymbol{V}' = [V'_{b1}, V'_{b2}, V'_{b3}]^{\mathsf{T}}$ be the voltage at each port of the shaded network in Fig. 2(b), and $\boldsymbol{I}' = [I'_{b1}, I'_{b2}, I'_{b3}]^{\mathsf{T}}$ be the current at each port. It follows that

$$\boldsymbol{I}' = \mathbf{Y}_b \begin{bmatrix} 0 \\ 0 \\ V'_{s3} \end{bmatrix} = V'_{s3} \begin{bmatrix} y_{b,13} \\ y_{b,23} \\ y_{b,33} \end{bmatrix}, \tag{9}$$

and

$$\boldsymbol{V}' = V'_{s3} \begin{bmatrix} -Z_0 y_{b,13} \\ -Z_0 y_{b,23} \\ 1 - Z_{m3} y_{b,33} \end{bmatrix}. \tag{10}$$

So

$$\begin{cases} \boldsymbol{a}'_b = \begin{bmatrix} a'_{b1} \\ a'_{b2} \\ a'_{b3} \end{bmatrix} = \dfrac{V'_{s3}}{2\sqrt{Z_0}} \begin{bmatrix} 0 \\ 0 \\ 1 - (Z_{m3} - Z_0) y_{b,33} \end{bmatrix}, \\ \boldsymbol{b}'_b = \begin{bmatrix} b'_{b1} \\ b'_{b2} \\ b'_{b3} \end{bmatrix} = \dfrac{V'_{s3}}{2\sqrt{Z_0}} \begin{bmatrix} -2Z_0 y_{b,13} \\ -2Z_0 y_{b,23} \\ 1 - (Z_{m3} + Z_0) y_{b,33} \end{bmatrix}. \end{cases} \tag{11}$$

Then, by definition,

$$\begin{cases} S_{13} = S_{31} = \dfrac{b'_{b1}}{a'_{b3}} = \dfrac{-2Z_0 y_{b,13}}{1 - (Z_{m3} - Z_0) y_{b,33}}, \\ S_{23} = S_{32} = \dfrac{b'_{b2}}{a'_{b3}} = \dfrac{-2Z_0 y_{b,23}}{1 - (Z_{m3} - Z_0) y_{b,33}}, \\ S_{33} = \dfrac{b'_{b3}}{a'_{b3}} = \dfrac{1 - (Z_{m3} + Z_0) y_{b,33}}{1 - (Z_{m3} - Z_0) y_{b,33}}. \end{cases} \tag{12}$$

Inserting (12) back to (7) yields

$$S_{21,\mathrm{cal}} = -2Z_0 \frac{y_{b,23}}{y_{b,33}} y_{b,13}. \tag{13}$$

As (13) is unrelated to any voltage or current, the equality should hold independent of means of excitation. Therefore, we turn on V_{s1}, and set $V'_{s3} = 0$. According to (2), the coil current $I_{b3} = V_{s1} y_{b,31} = V_{s1} y_{b,13}$. Writing $V_{s1} = 2\sqrt{Z_0} \times a_{b1}$, we have

$$S_{21,\mathrm{cal}} = -\sqrt{Z_0} \frac{I_{b3}}{a_{b1}} \frac{y_{b,23}}{y_{b,33}}. \tag{14}$$

Therefore, $S_{21,\mathrm{cal}}$ is proportional to the coil current I_{b3}. The ratio is

$$\begin{aligned} K(\mathrm{j}\omega) &= \frac{S_{21,\mathrm{cal}}}{I_{b3}} = -\frac{\sqrt{Z_0}}{a_{b1}} \frac{y_{b,23}}{y_{b,33}} \\ &= \frac{\sqrt{Z_0}}{a_{b1}} \cdot \frac{\begin{vmatrix} Z_{t1} + \mathrm{j}\omega L_1 & R_{13} + \mathrm{j}\omega M_{13} \\ R_{21} + \mathrm{j}\omega M_{21} & R_{23} + \mathrm{j}\omega M_{23} \end{vmatrix}}{\begin{vmatrix} Z_{t1} + \mathrm{j}\omega L_1 & R_{12} + \mathrm{j}\omega M_{12} \\ R_{21} + \mathrm{j}\omega M_{21} & Z_{t2} + \mathrm{j}\omega L_2 \end{vmatrix}} \end{aligned} \tag{15}$$

due to the relation $\mathbf{Y}_b = \mathbf{Z}_b^{-1}$. Note that Z_{t3} and L_3 vanish in (14), (15). It makes sense as probe measurements are expected to measure the coil current accurately enough irrespective of coil inductance or coil termination.

4) Simplifying (15)

Now we simplify (15). According to assumption (ii), $M_{12} = M_{21}$. According to assumptions (v), (vi), (vii), all $R \approx 0$, $L_1 = L_2$, $M_{13} \approx M_{23}$. Replacing $\mathrm{j}\omega$ by s, (15) simplifies to $K(s) = \sqrt{Z_0} a_{b1}^{-1} (L_1 + M_{21})^{-1} s/(s - p)$, where $p = -Z_0/(L_1 + M_{21})$. This is the transfer function of a first-order high-pass filter [12]. Its amplitude grows linear with frequency from 0 and phase drops linearly with frequency from $-\pi/2$, i.e.,

$$K(\mathrm{j}\omega) \approx \mathrm{j}\omega\kappa \mathrm{e}^{\mathrm{j}\omega\tau} \tag{16}$$

where $\kappa < 0$, $\tau < 0$ are constants specific to a setup. In the frequency domain, (16) is valid much until $|p| = Z_0/(L_1 + M_{21})$ rad, at which the amplitude of $s/(s - p)$ drops to $1/\sqrt{2} \times$ the linear approximation by (16) [12].

This concludes the derivation of the relation between S_{21} and coil current.

III. Methods

A. Numerically verifying S_{21}-coil current relation

To verify that $S_{21,\mathrm{cal}}/I_{b3}$ can be described by (15), models for simulation as shown in Fig. 4(c) is built in CST Microwave Studio (Dassault Systèmes, Paris, France). Copper coils of loop diameters 8.5 cm, 6.5 cm, 4.5 cm and 2.5 cm, of wire radius 0.4 mm (area 0.5 mm^2), segmented by capacitors of 5.6 pF into 2–4 pieces, is placed 2 mm above a sphere of 100 mm radius of biological tissue equivalent with $\varepsilon_r = 88.05 - \mathrm{j}382.6$ at 32 MHz, $\varepsilon_r = 63.93 - \mathrm{j}103.4$ at 128 MHz and $\varepsilon_r = 57.82 - \mathrm{j}45.96$ at 298 MHz [13]. Two H-field probes, one of ⌀2.6 cm loops, and the other of ⌀1.3 cm loops, are put above the coil. The probes are modelled as simple wire loops [7] instead of shielded loops to reduce computational costs. The effect of shielding can be modelled by connecting coaxial cables to the three-port network [7], as shown in Fig. 2(f). To evaluate $S_{21,\mathrm{cal}}/I_{b3}$, ports 1 and 2 are terminated by 50 Ω, port 3 is terminated by an arbitrary circuit load Z_{m3}, and $S_{21,b}$ and I_{b3} are simulated. The calibrated $S_{21,\mathrm{cal}}$ is taken as the raw $S_{21,b}$ minus $S_{21,a}$ with port 3 disconnected. The **S** parameters are then converted to **Z** parameters to get (15) [9, Sec. 4.4].

The setups are simulated up to 300 MHz to cover all nucleic resonance up to 7 T ($\omega_{\mathrm{r}} \leq 2\pi \times 298.0$ MHz).

B. Experiments

To demonstrate the use of the calibration method, a probe of two ⌀2.6 cm loops optimally overlapped at 32.1 MHz is used to measure preamplifier decoupling and active detuning. The experimental setup is shown in Fig. 1. A coil loop of 85 mm diameter is made of copper wire with 0.5 mm^2 cross-section area and terminated by a matching network. Since the coil is only for signal reception of ^{13}C and ^{23}Na, to avoid interference with ^{1}H imaging, a ^{1}H trap is installed on the coil. The current levels at the resonant frequencies of ^{13}C (30.99 MHz) and ^{23}Na (32.59 MHz) should equal, with a

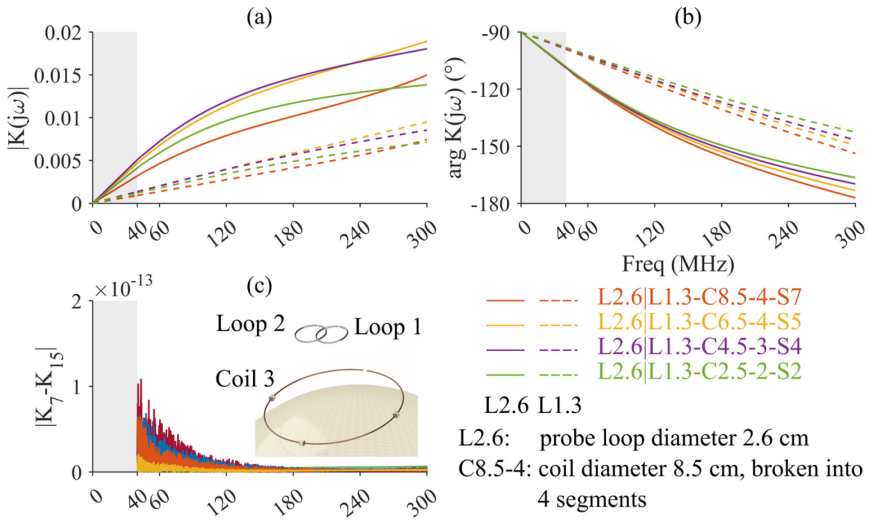

Fig. 4. Plots of $K(\mathrm{j}\omega)$ as calculated from simulated data. Data are simulated in 40–300 MHz range and extrapolated linearly down to 0 Hz. The resonant frequencies of coils are: C2.5-2: 291.0 MHz; C4.5-3: 287.9 MHz; C6.5-4: 274.7 MHz; C8.5-4: 231.8 MHz. (a) $|K(\mathrm{j}\omega)|$ as calculated from $|S_{21,\mathrm{cal}}|/I_{\mathrm{coil}}$ where $|S_{21,\mathrm{cal}}|$ is defined by (7). $|K(\mathrm{j}0)| = 0$. (b) $\arg K(\mathrm{j}\omega)$ defined the same way as in (a). As $\omega \to 0$, $\arg K(\mathrm{j}\omega) \to -90°$. (c) Difference between $K(\mathrm{j}\omega)$ defined by (15)—denoted as K_{15}, and $K(\mathrm{j}\omega)$ defined the same way as in (a)—denoted as K_7. $\max|K_7 - K_{15}| < 2 \times 10^{-13}$.

TABLE I
ERRORS BY LINEAR APPROXIMATION OF (16)

Configuration	63.9 MHz		128 MHz		298 MHz	
	Mag	Arg	Mag	Arg	Mag	Arg
L2.6-C8.5-4-S7	2.3	0.4	21.4	5.5	56.9	29.7
L2.6-C6.5-4-S5	2.9	0.5	24.2	5.8	81.6	31.0
L2.6-C4.5-3-S4	2.8	0.5	26.7	6.2	103.2	33.0
L2.6-C2.5-2-S2	3.3	0.5	28.4	6.4	116.3	34.2
L1.3-C8.5-4-S7	0.1	0.1	0.3	0.4	6.9	2.6
L1.3-C6.5-4-S5	<0.1	0.1	1.6	<0.1	6.4	3.3
L1.3-C4.5-3-S4	0.4	<0.1	3.8	0.3	19.4	4.8
L1.3-C2.5-2-S2	0.5	<0.1	4.8	0.5	26.3	5.5

All data are in percent. For the meaning of "Lx-Cx-x-Sx", refer to Fig. 4. Linear approximation is done by fitting data in 50–55 MHz range. Magnitude and phase are fitted separately. The constant terms are set to 0 or -90°. Errors less than 0.5‰ is displayed as "<0.1".

local minimum around the central frequency 31.79 MHz. The ^{1}H trap should to be tuned to 123.22 MHz. The probe is connected to a ZNL3 VNA (Rohde & Schwarz, Munich, Germany), of which output power is set -8 dBm and the IF bandwidth is set 10 kHz. The number of averaging is 100. The probe is 5 cm above the coil.

According to (16), the amplitude of the coil current can be approximated by $|I_{b3}| \approx |S_{21,\mathrm{cal}}|/\omega$. To avoid $|S_{21,\mathrm{cal}}|/\omega$ yielding data out of the displayable range of the VNA, we define the frequency-independent $S_{21,\mathrm{fi}}$ as

$$S_{21,\mathrm{fi}} = S_{21,\mathrm{cal}} \times \omega_a/\omega, \tag{17}$$

where ω_a is chosen $2\pi \times (80\ \mathrm{MHz})$ in this case.

IV. RESULTS

The magnitude and phase of the exact $K(\mathrm{j}\omega) = S_{21,\mathrm{cal}}/I_{\mathrm{coil}}$ using $S_{21,\mathrm{cal}}$ specified by (7) are plotted in Fig. 4(a), (b). The difference between this $K(\mathrm{j}\omega)$ and $K(\mathrm{j}\omega)$ as specified by (15) is plotted in Fig. 4(c). The maximum difference is below 2×10^{-13}, demonstrating the efficacy of (15).

The magnitude and phase of $K(\mathrm{j}\omega)$ are closely linear with frequency in the low frequency range, as predicted by (16). For different simulation setups, apparent deviation from a linear trend occurs at different frequencies. The difference between linear extrapolation from the curve parts in 50–55 MHz and $K(\mathrm{j}\omega)$ as predicted by (15) is shown in Table I. For the probe of ⌀2.6 cm, the frequency relation deviates fast from the linear relation of (16); for the probe of ⌀1.3 cm, the linear relation deviates much slower. $K(\mathrm{j}\omega)$ also deviates faster when the probe is nearer to the coil.

The measured preamplifier decoupling and active decoupling are plotted in Fig. 5. The calibrated $|S_{21,\mathrm{cal}}|$ curves are plotted in Fig. 5(a) and magnified in Fig. 5(b) and Fig. 5(c). The frequency-independent $|S_{21,\mathrm{fi}}|$ curves defined by (17) are plotted in Fig. 5(d). Before calibration, the measurements are severely affected by the probe crosstalk, as shown in Fig. 5(a). After calibration, the sensitivity for both probes improves to approx. -120 dB, almost the detection limit of the VNA [14]. Without the calibration, the true shape of coil current is buried under the probe's crosstalk. The $|S_{21,\mathrm{fi}}|$ curves give the frequency of the maximum preamplifier decoupling, the maximum active detuning and the ^{1}H trap as 31.98 MHz, 33.10 MHz, and 124.24 MHz, respectively. Active detuning and ^{1}H trap circuits are not perfectly tuned to their assigned frequencies in this case. The coil current values at the resonance frequencies of ^{13}C and ^{23}Na are -66.2 dB and -67.0 dB, respectively, differing only by 0.8 dB. Active detuning suppresses coil current further by 17.2 dB and 24.8 dB for ^{13}C and ^{23}Na, respectively.

V. DISCUSSION

A. Probe construction and measurement

Step 1 of Section I instructs keeping the probe far from the coil when measuring coil current. However, the received signal becomes feeble when the probe is too far. Thus, there is an optimal range of coil-to-probe distance. This range depends on loop size, coil size, RF power of the VNA, etc. There is no universal number for the optimal range. In practice, though, putting the probe too close results in S_{21} distortion, and putting the probe too far weakens signal, as shown in Fig. 6(a). Both are immediately noticeable on a VNA screen, and the range evaluation takes merely a few seconds.

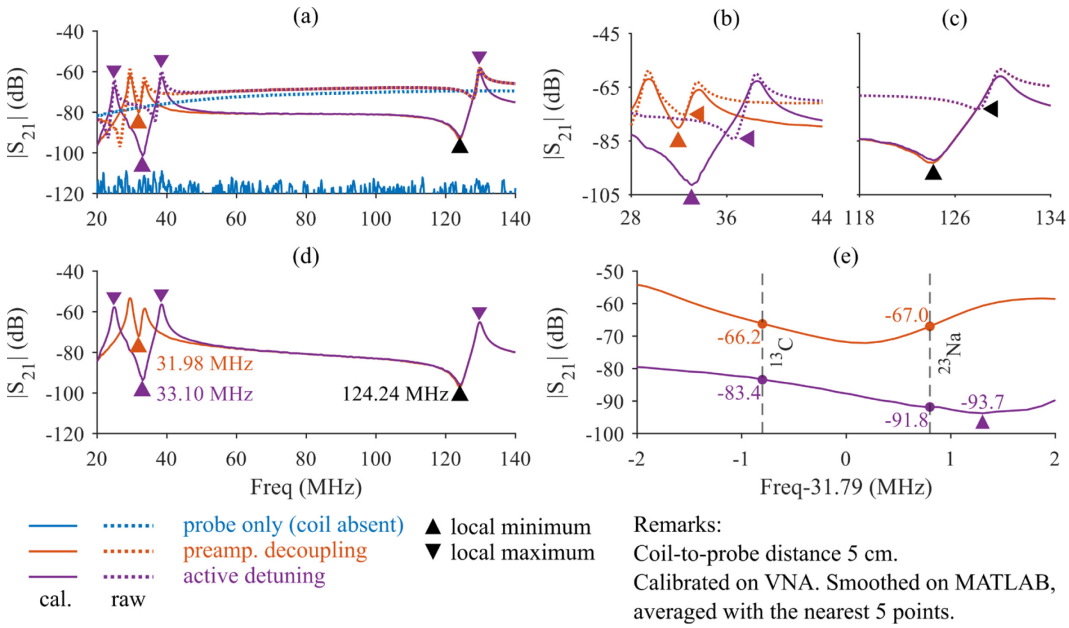

Fig. 5. Smoothed measured curves of preamplifier decoupling and active detuning. (a) Raw $|S_{21,b}|$ and calibrated $|S_{21,\mathrm{cal}}|$ measurements. (b), (c) Calibrated and raw measurements in 28–44 MHz and 118–134 MHz. ▲ and ◀ mark the minima of calibrated and raw measurements, respectively. (d) $|S_{21,\mathrm{fi}}|$ rid of frequency dependency as defined by (17). The $|S_{21,\mathrm{fi}}|$ curves differ noticeably from the $|S_{21,\mathrm{cal}}|$ curves. The minima of $|S_{21,\mathrm{cal}}|$ and $|S_{21,\mathrm{fi}}|$ are at the same frequencies. (e) $|S_{21,\mathrm{fi}}|$ curves near 31.79 MHz. The active detuning is not tuned to 31.79 MHz in this case, leaving an 8.4 dB current difference between ^{13}C and ^{23}Na frequencies. Because active detuning is off during signal reception, active detuning need not be equal at ^{13}C and ^{23}Na frequencies.

It is also instructed to keep the coil far from the sample; otherwise, the calibration fails, as shown in Fig. 6(b).

As shown in Table I, $K(\mathrm{j}\omega)$ of the smaller probe is highly linear in a wider frequency range. This confirms the prediction in Section II.D.4): a smaller probe has lower L_1, so the upper bound of linearity $Z_0/(L_1 + M_{21})$ goes higher. This suggests that, if a higher cutoff frequency of linear approximation is desired, smaller probes should be used.

B. Frequency linearity of $K(j\omega)$

In the experiment of Section III.B, the loop diameter of the probe is 2.6 cm. Deviation of the magnitude from (16) is at least 25.2%, according to Table I. Therefore, in this experiment, around 124 MHz, it is inaccurate to remove frequency dependency by (17). However, in practice, traps are only required to block current strongly enough so that no artefact is left on MR images [15], and precise tuning is not needed. Moreover, the resonant frequencies of ^{1}H trap as found by $|S_{21,\mathrm{cal}}|$ and $|S_{21,\mathrm{fi}}|$ are nearly the same, differing by less than 140 kHz, or 1.1 ‰ of 124.24 MHz. The calibration suffices for practical use even with $|S_{21,\mathrm{cal}}|$ only.

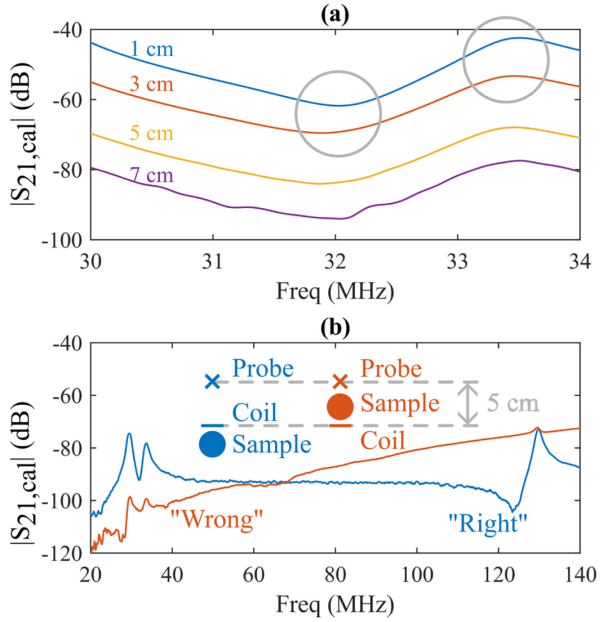

Fig. 6. (a) The experiment setup in Section III.B measured with coil-to-probe distances of 1, 3, 5, 7 cm. 1 cm coil-to-probe distance causes $|S_{21}|$ distortion as circled out. At 7 cm distance, $|S_{21}|$ signal becomes too weak. (b) Keeping the distance 5 cm but with samples at different positions. The probe must not be near the sample.

Note that, as long as assumptions (i)–(iv) are satisfied, at each frequency, $S_{21,\mathrm{cal}}$ is proportional to the coil current I_{coil}. For most cases of MRI coil building, it suffices for current-suppression circuits to be tuned to only one or several discrete frequencies. To fine-tune circuits, it suffices to have $S_{21,\mathrm{cal}} \propto I_{\mathrm{coil}}$. As discussed previously, even if S_{21}/I_{coil} deviates from (16), fine-tuning is essentially unaffected. In these cases, the calibration procedure that consists only of steps 1–4 in Section I can be used up to 300 MHz.

Experimental validation of (14), (15) requires a three-port VNA, and a current meter to measure coil current I_{b3} in a wide band. Because of the special peripheral devices needed, this article is limited to validating (14), (15) by simulation.

VI. Conclusion

A calibration method of double-loop measurement of coil current is described. It is shown mathematically that the calibrated S_{21} is proportional to the coil current. The effect of sensitivity improvement and removal of frequency dependency are demonstrated experimentally. Practical guidelines for accurate probe measurement are suggested. The proven S_{21}-current relation serves as a basis for fast, accurate probe measurements. It enables designers to accurately fine-tune circuits for current suppression such as active detuning circuits and traps in a wide frequency range relevant to MRI.

REFERENCES

[1] P. B. Roemer, W. A. Edelstein, C. E. Hayes, S. P. Souza, and O. M. Mueller, "The NMR phased array," *Magn Reson Med*, vol. 16, no. 2, pp. 192–225, Nov. 1990, doi: 10.1002/mrm.1910160203.

[2] L. Darrasse and G. Kassab, "Quick measurement of NMR-coil sensitivity with a dual-loop probe," *Review of Scientific Instruments*, vol. 64, no. 7, p. 1841, Sep. 1998, doi: 10.1063/1.1144020.

[3] A. Haase *et al.*, "NMR Probeheads for In Vivo Applications," *Concepts Magn Reson*, vol. 12, no. 6, pp. 361–388, 2000, doi: https://doi.org/10.1002/1099-0534(2000)12:6%3C361::AID-CMR1%3E3.0.CO;2-L.

[4] J. D. Sanchez-Heredia *et al.*, "RF coil design for accurate parallel imaging on 13C MRSI using 23Na sensitivity profiles," *Magn Reson Med*, vol. 88, no. 3, pp. 1391–1405, Sep. 2022, doi: 10.1002/MRM.29259.

[5] W. Wang, J. D. Sanchez-Heredia, V. Zhurbenko, and J. H. Ardenkjaer-Larsen, "Condition for Optimal Preamplifier Decoupling in One-turn Single- and Multi-gap Shielded Loop MRI Detectors," in *2022 IEEE 2nd Ukrainian Microwave Week, UkrMW 2022 - Proceedings*, IEEE, 2022, pp. 150–154. doi: 10.1109/UkrMW58013.2022.10037007.

[6] W. Wang, V. Zhurbenko, J. D. Sánchez-Heredia, and J. H. Ardenkjær-Larsen, "Trade-off between preamplifier noise figure and decoupling in MRI detectors," *Magn Reson Med*, vol. 89, no. 2, pp. 859–871, Feb. 2023, doi: 10.1002/mrm.29489.

[7] M. D. Harpen, "The Theory of Shielded Loop Resonators," *Magn Reson Med*, vol. 32, no. 6, pp. 785–788, 1994, doi: 10.1002/mrm.1910320615.

[8] L. L. Libby, "Special Aspects of Balanced Shielded Loops," *Proceedings of the IRE*, vol. 34, no. 9, pp. 641–646, 1946, doi: 10.1109/JRPROC.1946.230887.

[9] D. M. Pozar, *Microwave Engineering*, 4th ed. Singapore: John Wiley & Sons, Inc., 2011.

[10] S. M. Wright, "Receiver Loop Arrays," in *RF Coils for MRI*, J. T. Vaughan and J. R. Griffiths, Eds., John Wiley & Sons, Inc., 2012, pp. 65–80.

[11] K. Kurokawa, "Power Waves and the Scattering Matrix," *IEEE Trans Microw Theory Tech*, vol. 13, no. 2, pp. 194–202, Mar. 1965, doi: 10.1109/TMTT.1965.1125964.

[12] A. S. Sedra and K. C. Smith, "11.4 First-order and Second-Order Filter Functions," in *Microelectronic Circuits*, 4th ed.New York: Oxford University Press, Inc., 1998, pp. 900–908.

[13] C. Gabriel, "Compilation of Dielectric Properties of Body Tissue at Microwave Frequencies," U.S. Air Force, Brooks Air Force Base, Texas, 1996. [Online]. Available: https://apps.dtic.mil/docs/citations/ADA309764

[14] "R&S®ZNL vector network analyzer | Rohde & Schwarz." https://www.rohde-schwarz.com/dk/products/test-and-measurement/network-analyzers/rs-znl-vector-network-analyzer_63493-432704.html (accessed Aug. 11, 2022).

[15] A. Kocharian, P. J. Rossman, T. C. Hulshizer, J. P. Felmlee, and S. J. Riederer, "Determination of appropriate RF blocking impedance for MRI surface coils and arrays," *Magnetic Resonance Materials in Physics, Biology and Medicine*, vol. 10, no. 2, pp. 80–83, Jun. 2000, doi: 10.1016/S1352-8661(00)00071-5.